International Journal of Applied Sciences: Current and Future Research Trends
(IJASCFRT)
ISSN: 2790-3990
https://ijascfrtjournal.isrra.org/index.php/Applied_Sciences_Journal

MXenes in Gas Sensing

Vir Gogia[a], Aarav Doshi[b], Aamir Akbar Khan[c], Sananjay Biswas[d*]

[a,b,c]*Dhirubhai Ambani Internation School, Mumbai, 400098, India*
[a,b,c,d]*Pion Academy, Shiv Smriti Chambers, Dr Annie Besant Road, Bhim Nagar, Worli, Mumbai, 400018, India*
[d]*Email: sananjayb@gmail.com*

Abstract

An extensive review of the history and current status of MXene-based gas sensors is presented here. The unusual electrical, optical, and mechanical features of MXenes, a novel family of two-dimensional transition metal carbides and nitrides, have garnered a lot of attention in recent years. These properties make MXenes highly promising materials for various applications, including gas sensing. This review examines various strategies used to enhance the performance of MXene-based gas sensors, including surface modification, hybridization with other materials, and device design. A detailed analysis of the sensing mechanism and the factors that influence the sensing performance is also presented. The authors also address the challenges and limitations MXene-based gas sensors face, including low stability and sensitivity, poor selectivity, and limited applicability to different gas types. They highlight the need for further research to overcome these limitations and enhance the sensing performance. The review provides valuable insights into the potential and limitations of MXene-based gas sensors and serves as a useful reference for researchers and engineers working in the field. This study is concluded by highlighting the future directions and opportunities for further development of MXene-based gas sensors.

Keywords: MXene; gas-sensor; gas concentration; sensitivity.

1. Introduction

MXenes, a two-dimensional material discovered in 2011, has attracted a great deal of attention in various applications due to their unique physical and chemical properties MXenes have a three-dimensional network of carbon atoms, making them a promising sensor material with abundant gas adsorption active sites [1]. Electrochemical energy storage and conversion, electromagnetic shielding, wearable sensors, and personal thermotherapy are all areas where MXenes have shown promise because of their metallic conductivity and pseudocapacitive nature [2].

Received: 3/15/2025
Accepted: 5/2/2025
Published: 5/9/2025

---

* Corresponding author.

MXenes are attractive for gas sensing because of their exceptional stability, metallic conductivity, and variable surface chemistry [3-5]. MXenes also have a number of advantageous properties, such as high flexibility, convenient solution processability, and easy functionalization, which make them good candidates for making composites with other nanomaterials [6-8] . This is exemplified by the composite prepared by Qingting Li and his colleagues [1], which was composed of MXene layers and loosely stacked $Fe_2(MoO_4)_3$ nano-layers . Due to its large surface area of 47.0 m^2/g, the composite had improved gas sensing properties, with a response of 43.1% to 100 ppm n-butanol and a response and recovery time of 18/24 s. MXene is modified by two-dimensional transition metal dichalcogenides, such as doping, surface treatment, alkali treatment, carbon-based materials, and two compounds. In addition, an intercalator, such as Na^+, K^+, Mg^{2+}, Li^+, Sn^{4+}, or Mn^{2+}, is added to increase the interlayer spacing. The intercalator can be regarded as a pillar that keeps the distance between layers, and metal cations can be spontaneously inserted into the MXene layer [9], thereby increasing the interlayer spacing. However, because fluorine terminal has negative impacts on MXene's performance, a fluoride-free synthesis technique is required. As a result, many new preparation methods have been researched to solve the problems of agglomeration and yield.

MXenes are a unique class of layered materials that have recently been extensively studied for their potential in a wide range of applications. MXenes are composed of two main layers, $Ti_3C_2O_2$ and $Ti_3C_2(OH)_2$, and an intercalator that helps to increase the distance between the layers. DMSO is the most frequently used intercalator for MXenes and it is known to embed in $Ti_3C_2O_2$ and $Ti_3C_2(OH)_2$ to increase the interlayer spacing layers [5].The theoretical model of DMSO that was embedded in $Ti_3C_2O_2$ and $Ti_3C_2(OH)_2$ shows that the interlayer spacing of $Ti_3C_2(OH)_2$ is larger than that of $Ti_3C_2O_2$. This suggests that $Ti_3C_2(OH)_2$ and DMSO mutually exclusive compounds produce a larger interlayer spacing than $Ti_3C_2O_2$. MXenes have a small interlayer spacing due to the in-plane covalent bond and the van der Waals force between the layers. In addition to increasing the specific surface area, active sites, and ion transport channels, increasing the interlayer gap between the $Ti_3C_2(OH)_2$ and DMSO layers eliminates hydrogen atoms from both materials. This makes MXenes remain dispersed and allows them to form a heterogeneous p–n junction with a built-in electric field at their interface. An increase in conductivity is observed in the composite material's sensor when it is exposed to NO_2 because gas molecules adsorb on its surface and steal electrons. Because of the p-n junction's inherent electric field, electron transport is impeded until the Fermi level is at the same potential. At this point, the Schottky barrier forms. When Al and Li are combined to make Al-Li alloy, their volumes are said to increase by more than 100 percent. This enlargement allows the interlayer binding force to be lowered, allowing the Al layer to be detached from the MAX(Mn+1AXn) Using the intercalation-alloying-expansion- micro explosion process, Sun and his colleagues successfully fabricated single-layer and few-layer fluorine-free Ti_3C_2Tx. Al-Li alloy was created when Li^+ ions from the electrolyte were pushed deeper into the Al layer of MAX by the electric field. Then the Al-Al layer expanded H_2 would be produced as a by-product of the Al-Li layer reacting with H_2O upon submerging litigated MAX in water [10]. After a micro explosion transpired in the space between the layers, MAX peeled off into Ti_3C_2Tx nanosheets (Fig. 1). It was helpful in accomplishing the actual manufacture of MXene because the Ti_3C_2Tx generated by this process had an ultra-thin transparent structure, a high yield, and a quick speed.

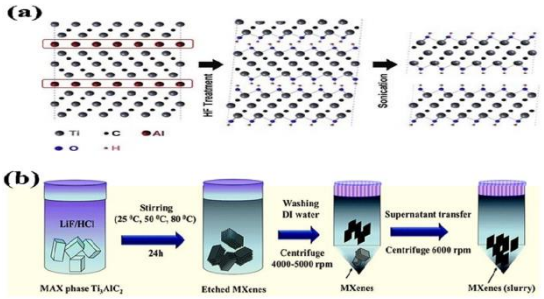

Figure 1: (a) Ti_3C_2Tx synthesized by HF etching [11];(b) Ti_3C_2Tx synthesized by HCl + LiF etching

Experimental Work

MXene-based gas sensors offer many advantages over traditional gas sensors, making them an attractive option for gas detection. MXenes are a class of two-dimensional materials that possess unique optical and electronic properties that make them suitable for use in optical and electronic gas sensors. These materials are highly sensitive to a variety of gases, making them ideal for detecting even low concentrations of gases [13]. Additionally, MXenes are relatively inexpensive and easy to prepare, making them more cost-effective than many other gas sensors. Furthermore, MXenes have a high surface area-to-volume ratio, allowing them to detect gases quickly and accurately. Finally, MXenes are also lightweight, making them easy to transport and deploy in a variety of environments. These advantages make MXenes an attractive option for gas detection and make them a promising material for gas sensors. The two-dimensional (2D) layered nanomaterials MXenes exhibit remarkable physiochemical properties that cater to numerous applications in energy conversion and storage. Besides, their layer-spacing tunability allows for structural and surface engineering of MXenes to enhance their physicochemical properties. The gas-sensing properties of MXenes depend on their interlayer swelling, which results from adsorption, charge transfer, and chemical reaction of the target gas[7] [8] . Therefore, improving the MXenes' structure and surface chemistry is an effective method to improve their sensing performance. Also, the MXenes' have received a lot of attention for applications in energy conversion, catalysis, and electronics. However, their application to gas sensors has not yet been fully explored. The objective of this literature review is to present a comprehensive overview of strategies and pros and cons of MXene-based gas sensors in order to provide guidance for future development. During the past few years, MXenes have emerged as attractive two-dimensional (2D) transition metal carbides and nitrides with many novel properties, such as graphene-like morphology, high thermal and electrical conductivity, large surface-to-volume ratio, mechanical flexibility, and great hydrophilic surface functionalities. This makes MXenes highly suitable for gas sensing applications due to their ability to effectively harness their morphology and interlayer structures. Moreover, MXenes can efficiently form nanohybrids with other nanomaterials to revamp their sensing performance and improve gas-sensing applications.

1.1 Synthesis of MXenes

The two-dimensional (2D) layered materials known as MXene are made up of early transition metal carbides and/or nitrides **(Fig.2)**. They are hydrophilic, have large surface area, and tunable electronic and optical properties. Photodetectors, flame-retardant polymer materials, water purification, energy conversion and storage,

sensors, EMI shielding, gas separation, medicinal imaging and treatment, and catalysis are just a few of the many fields that benefit from their use. Several strategies for the synthesis of MXenes have been developed, namely, etching, delamination, and hybridization with 2D nanomaterials[14-15]. The synthesis process can influence the properties of the resulting MXenes, such as their electrical conductivity, structural, morphology, and oxidation stability.

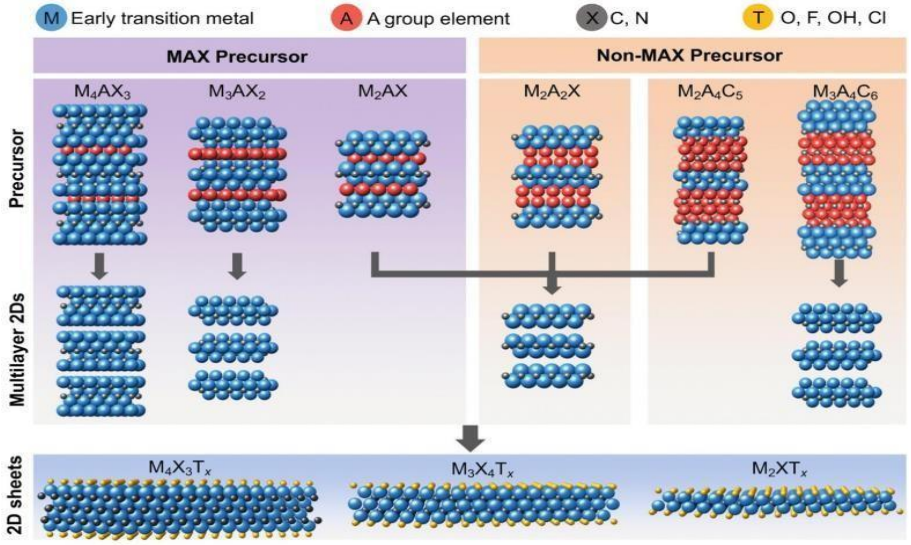

Figure 2: Top-down selective etching synthesis of MXenes from MAX and non-MAX precursors. Two-dimensional (2D) multilayer powders (termed multilayer 2Ds) and 2D sheets of the three MXTx kinds (M_2XTx, M_3XTx, and M_4XTx) are both synthesizable. Multilayer powders on the 2nd dimension feature surface terminations that are analogous to those of 2D sheets. For the sake of clarity, layered 2D powder surfaces are not depicted [16].

The synthesis of MXenes is typically a complex procedure that includes a variety of techniques and a lot of work. For example, a strong acid-fluoride etching method requires high concentrations of fluoride salt and strong acids, which are hazardous to human health and the environment. In addition, MXene sheets etched by the traditional HF process often contain large amounts of chemical inert-F terminal groups [17]. In order to minimize the harmful effects of fluoride salts, some researchers have introduced alternative synthesis processes for producing MXenes. For example, a group of researchers prepared Ti_3C_2Tx MXenes using an in-situ etching technique that does not require a fluoride reagent[18]. The results of this study indicate that a low concentration of fluoride can be used to etch the A atomic layers in MAX phases without adding a large amount of fluoride salts to the solution. This approach was applied to produce multilayer Mo_2CTx MXenes with a sensitivity of 0.0366 O/ppm at 140 ppm and a LOD of 220 ppb. The optimum concentration of the MXene and the sonication time were optimized to obtain this sensitivity and performance. However, this type of MXene synthesis does not guarantee an adequate level of oxidation stability and is susceptible to the presence of defective sites at the edges of the flakes [19]. In order to create a long-lasting, reliable MXene sensor, it is essential to carefully regulate the chemistry of the parent MAX phase, the etching conditions, the defect passivation, the dispersion medium, and the storage conditions. Mechanical exfoliation techniques are widely employed for the production of graphene, transition metal disulfides, transition metal oxides, and hexagonal boron nitrides [20]. Hydrofluoric

acid (HF), hydrochloric acid (HCl), lithium fluoride (LiF), and fluoride-free etching are some of the most used wet chemical production procedures for 2D MXenes **(Table 1) [21].**

Table 1: Methods for etching MXene with its corresponding conditions, procedures, benefits, and drawbacks.

S.No.	**Etching method**	**Procedure** **conditions**	**Advantages**	**Disadvantages**
1	40 % HF	Etching at room temperature	Simple operation	A very hazardous reactant, a broad etching range, and several impurity functional groups characterize the resulting product.
2	NH4HF2 (1 mol/L)	NH_4HF_2 (1 mol/L) as an etchant at room temperature,	Conditions are mild, and there is no danger to humans and animals.	Low product purity is the result of the product's inclusion of multiple by-products.
3	Molten fluoride salt/high Temperature	The mixture of fluoride salt and Ti_4AlN_3 powder under the Ar atmosphere,	Reaction conditions are more severe, and the procedure is difficult and potentially hazardous.	It is possible to produce an N-based MXene that is of high purity.
4	LiF + HCl	Exfoliation at 60 °C–180 °C	Etching is a simple process with non-hazardous reactants that may cover a wide area.	In many cases, the final product lacks essential components.
5	Generic Lewis acid etching	Generic Lewis acid combined with several A-element- containing MAX phases (Al, Zn, Si, Ga, etc.)	MXenes in their pure form have been shown to exhibit exceptional electrochemical performance and a sizable etching window.	As a result, the final product is impure.

1.2 Wet chemical etching methods

Wet chemical etching is an important technique to synthesize MXenes. The etching method is used to oxidize the surface of MXenes, which enhances their mechanical and electrical conductivity as well as reduces the defect density. The oxidation of MXenes is controlled through the choice of a suitable etching agent and the sonication time. Various etchants have been used for the synthesis of MXenes, including acid halogens, molten salts, and non- aqueous oxidizing agents. The etching method is influenced by the sensitivity and selectivity of MXene-based gas sensors. Several strategies and prognoses are available to control the sensitivity and selectivity of MXene-based sensors, such as modifying the surface functional groups and the interlayer spacing, as well as improving the transport between layers. The resultant gas- sensing devices can identify a wide range of Volatile organic compounds (VOCs), such as toluene, ethanol, and benzene, as well as other contaminants and prescription medications. The suggested hydrothermal etching approach made it possible to exfoliate MXenes in a way that was both environmentally friendly and highly efficient, showing promise for the easy preparation of 2D MXenes and opening the door to several potential uses [22]. An efficient bi-functional electrocatalyst for the water-splitting process may be created by focusing on the synthesis of basal plane-porous titanium carbide MXene, which is then employed as the effective host for integrating with known-catalytic active phase (IrCo) [23].establish that MXenes may be etched and delaminated in the presence of ammonium dihydrogen fluoride and organic polar solvents without the need of water . Research the novel and emerging group of 2D materials, namely MXene and its nanocomposites, with a focus on the synthesis of basal-plane-porous titanium carbide MXene, which is then used as an effective host for the incorporation of a known catalytically active phase (IrCo) as an effective bifunctional electrocatalyst toward water splitting. investigate the recently discovered 2D material MXene and its nanocomposite [23]. Due to their metallic conductance and many surface terminations, 2D MXenes are promising candidates as surface-enhanced Raman scattering (SERS) substrates. He and his colleagues [24,25,26].provide a simple method for synthesizing bimetallic solid-solution TiVC (MXene) for use in surface enhanced Raman scattering [27].

One of the main challenges in gas-sensing using MXenes is aggregation, which can significantly decrease their sensitivity and selectivity. Moreover, the adsorption of other molecules like water and adsorbents can also affect the gas-sensing performance of MXenes. Fortunately, MXenes can be successfully modified to minimize the adsorption and enhance their sensitivity by modifying the interlayer spacing. According to **Fig. 2a**, Feng and his colleagues [28]. employed ultrasonic-assisted HF acid etching to drastically cut down on etching time. Success in preparing Ti_3C_2 was achieved by Zhang and his colleagues [29]., utilizing a combination of HCl and LiF as the etchant. Scanning Electron Microscope (SEM) images of the deposition **(Fig. 2b and c)** reveal the typical morphology of Mexene with an accordion-like structure. Using the resulting stable suspension of delaminated $Ti_3C_2T_x$ flakes (the zeta potential is -8.2 mV), flexible, free-standing Ti_3C_2Tx paper were readily prepared by vacuum-assisted filtration. The morphologies of the $Ti_3C_2T_x$ papers are shown in **Fig. 2**. By controlling the concentration or volume of the stable suspensions, the thickness of the paper can range from several to dozens of micrometers. Cross-sectional SEM images of the paper reveal a well-aligned stacking structure throughout the entire paper **(Fig. 2(d)).** All of the $Ti_3C_2T_x$ papers show excellent flexibility and can be readily folded into various shapes without observable damage **(Fig. 2(e)).**

$$Ti2AlC + 6LiF+3HCl \rightarrow Ti2C +Li3AlF6 +3LiCl +3/2H2 \quad (1)$$

$$Ti2C + 2H2O \rightarrow Ti2\ C(OH)2 +H2 \quad (2)$$

$$Ti2C +2LiF +2HCl \rightarrow Ti2\ CF2 +2LiCl +H2 \quad (3)$$

Another approach to control the adsorption of different gases is to modify the resistance of MXenes. A-MoCl˙x MXenes with a higher resistance were found to be superior in terms of gas response and stability. They showed better p-type sensing characteristics, as well as multiple responses to acetone, ethanol, propanal, hexane, toluene, and NO2 in comparison to b-Mo2C. The a-MoC1˙x MXene-based sensor was also stable for a half-year at room temperature, and it offered an excellent selectivity toward toluene over other VOCs.

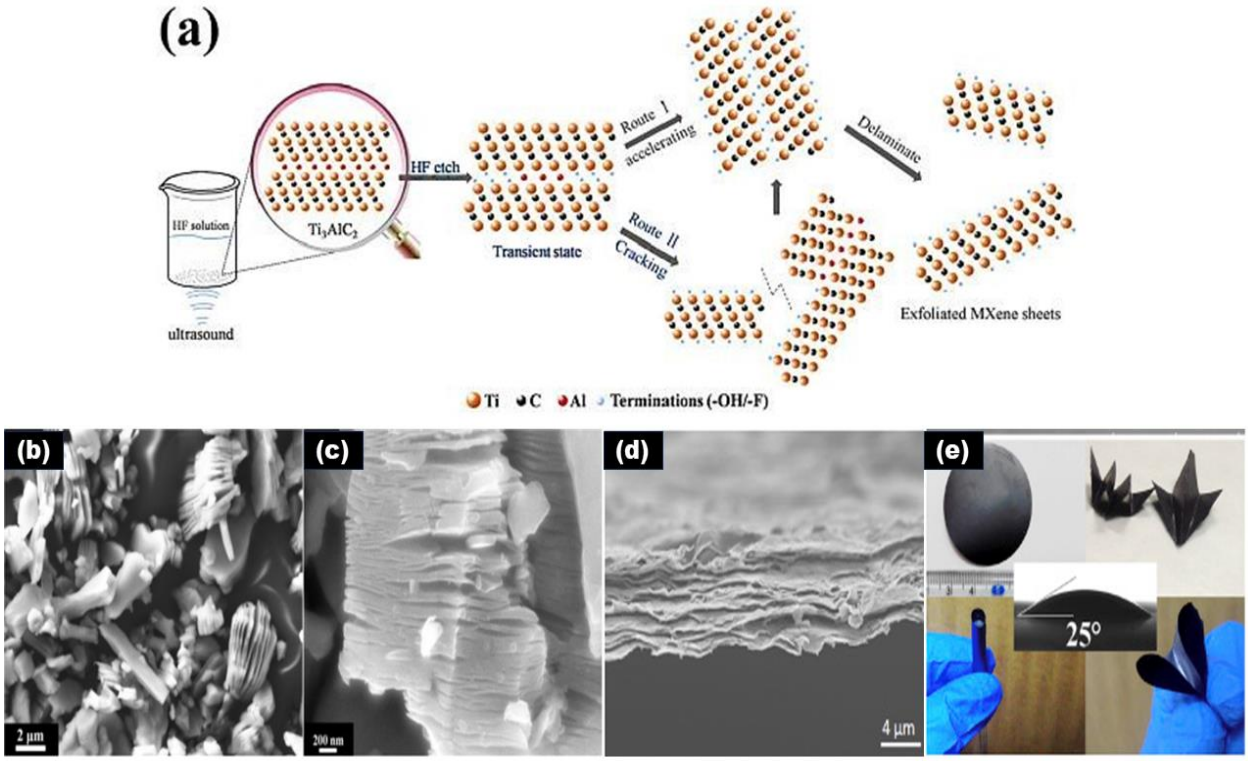

Figure 2: (a) Sonication speeds up the etching and delaminating process, as seen in this schematic;(b,c) SEM image of unexfoliated Ti_3C_2 grains, showing the 2D structure of Mxene [28]; (d) Cross-sectional SEM images of MXene paper under different magnifications showing its layer stacked structure with different thickness. (e) digital photographs of Ti_3C_2Tx films being folded into various shapes by fingers and wrapped around a 4-mm-diameter glass rod without breakage, showing its excellent flexibility. The middle image shows the contact angle (25°) of a water droplet on the surface, indicating its hydrophilicity [29].

1.3 Non-wet chemical etching method

High performance of MXene-based gas sensors depends on several factors, including the synthesis method,

precursor, and surface chemistry. These factors can be manipulated to improve the MXene gas-sensing performance. A minimal intensive layer delamination (MILD)-like etching process was used to produce MXene from Ti_3C_2Tx precursors with a hydroxyl or oxygen-terminated surface and low fluorine content. This etchant was also found to reduce the amount of defect formation and maintain the MXene lateral dimension. In addition, the morphology of the etched MXene films could be controlled to facilitate gas- sensing applications. The Co_3O_4@PEI/Ti_3C_2Tx MXene composites were fabricated by riveting Co_3O_4 nanocrystals to branched polyethyleneimine (PEI) functionalized Ti_3C_2Tx MXene sheets using a simple noncovalent chemical technique and a hydrothermal process[30]. Exciting new discoveries differentiate V_4C_3Tx as a similar material to the well-known Ti_3C_2 MXene, and the use of V_4C_3Tx for the first time in acetone detection may pave the way for further research into MXene potential uses in gas sensors [31]. With a working temperature of only 25^{o}C, a detection limit of 1 ppm (much lower than the 1.8 ppm diabetes diagnosis threshold), and a high selectivity towards acetone in a mixed gas of acetone and water vapor, a V4C3Tx-based acetone sensor shows promising performance for use in the much faster and earlier diagnosis of diabetes. Different HF contents (ranging from 30 wt% to 5 wt% at room temperature) were used to perform the MILD-like etching of Ti_3C_2Tx flakes. The result of the etching was that the MXene samples showed an accordion-like morphology with the interlayer spacing being trapped between Na+ ions and water molecules. The resulting morphology of the MXenes could be further optimized to enhance the gas-sensing performance by engineering their structural and surface chemistry. Exciting new results identify V_4C_3Txas a similar material to the well-known Ti_3C_2Tx, and the usage of V_4C_3TxMXene for the first time in the field of acetone detection may pave the way for the exploration of applications of MXene in gas sensors [32]. To address and improve upon the sensor drift problem, Dong et. al. [33]. suggest a unique memory method that may be used in conjunction with the conventional machine learning classifier. In order to control the defect formation of MXene flakes and maintain their lateral dimension, a number of strategies were developed. One strategy involves using different HF concentrations to obtain a wide range of d-spacings and the degree of intercalation between the Na^+ ions and water molecules, which would then be monitored with in situ X-ray diffraction. Another strategy focuses on modifying the gas-sensing properties of MXenes by incorporating interlayer spacers, such as hydroxyl or oxygen-terminated surfaces [27]. This strategy enables the MXenes to absorb and diffuse gases effectively. The interlayer spacers can also be used to modify the oxidation and reduction mechanisms of MXenes.

Moreover, the synthesis of MXenes with higher atomic-layer thicknesses and greater lateral dimensions is possible by using different etching methods. The resulting layered structures can be easily incorporated into MXene-based gas sensors to enhance their sensing capabilities and performance. MXene-based gas sensors are characterized by high sensitivity and selectivity to various gases, a large lateral dimension, strong hydrophilicity, and rich elemental compositions and surface terminations. These properties have made MXenes highly appealing for gas-sensing applications. However, more research is needed to increase the sensitivity and selectivity of MXene-based sensors and achieve higher performance.

1.4 Structure of MXenes

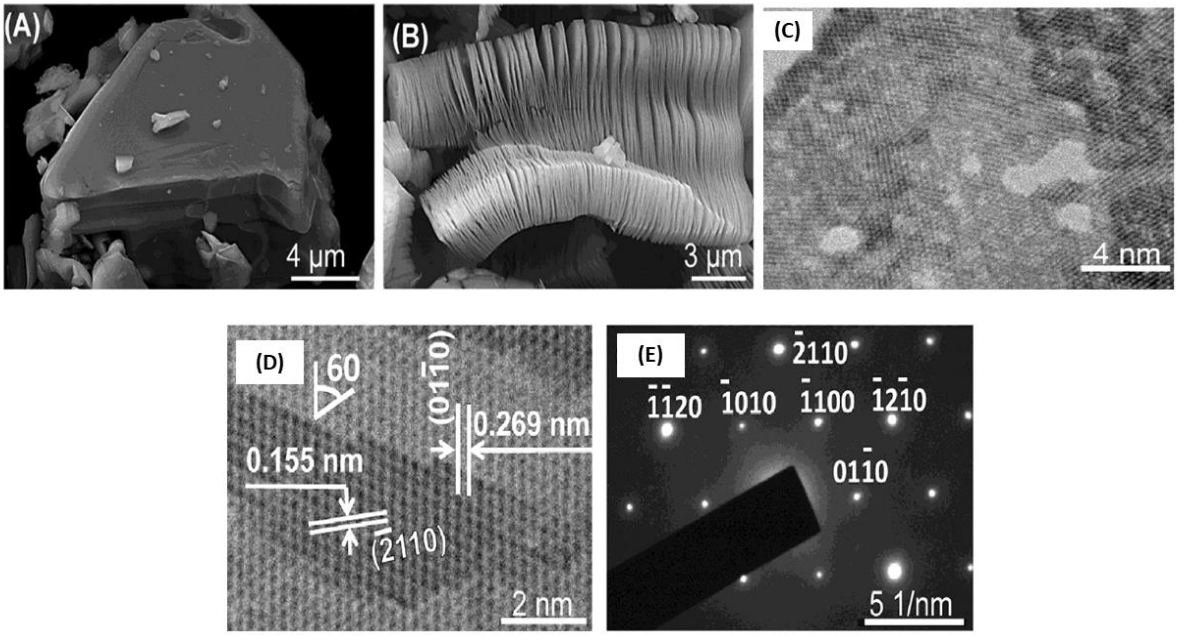

Figure 3: Micrographs taken using a scanning electron microscope (SEM) of MAX and MXene: (a) Ti_3AlC_2; (b) Ti_3C_2Tx; (c) TEM image Ta_4AlC_3 after HF treatment, (d) HRTEM of multilayer MXene, and (e) SAED[35].

MXene, or metal oxynitride, is a 2D material that resembles graphene in structure. Fig.**3a-b** displays scanning electron microscope (SEM) micrographs of the microstructures of several MXenes (Ti_3C_2Tx, Ti_2CTx, Ta_4C_3Tx, TiNbCTx, and Ti_3CNTx). Currently, Ti_3C_2Tx is the MXene material that has been the subject of the most study (70% of all MXene-related studies). Metal is removed from Ti_3AlC_2 to create Ti3C2Tx with void layers. Ti3C2Tx materials with distinct chemical and physical characteristics are obtained because the empty layer gap varies with etching conditions [34]. **Fig. 3d** shows a higher magnification high-resolution transmission electron microscope (HRTEM) image of a Ta_4C_3 layer with some nanometer sized holes. Similar atomic defects were reported in functionalized graphene. The latter can act as nucleation sites for metal oxides which are useful in many applications. HRTEM and selected area electron diffraction (SAED) **(Fig. 3e, f)**, however, show that the crystallinity of the basal planes of the MAX phases is preserved. These images confirm the hexagonal structure of the Ta_4C_3 layers. Measurements of the d spacings shown in the figure resulted in 0.269 and 0.155 nm for the (0110) and (2110) lattice planes, respectively. When these values are used to calculate a lattice parameter, the value obtained, 0.31 nm, is in excellent agreement with that of a parameter of the no exfoliated Ta_4AlC_3 MAX phase, viz. 0.311 nm.38 It is thus reasonable to conclude that the MAX crystal structure of the basal planes is maintained in the MXenes. The approach offered by Chen et. al. [36].is simple and applicable, and it may be used to create MXene-based gas-sensing devices with a response that is stable in air and in the presence of water. The high selectivity towards acetone in a mixed gas of acetone and water vapor and the low detection limit of 1 ppm (lower than the 1.8 ppm diabetes diagnosis threshold) demonstrate the good performance of a V_4C_3Tx based acetone sensor, which may find use in the much faster and earlier diagnosis of diabetes. With

these promising results, V_4C_3Tx MXene is clearly distinguished as a similar material to the well-known Ti_3C_2Tx [34], and its usage in acetone detection marks its first foray into the realm of MXene applications in gas sensors. Reference: Yang et. al. [23] present a concept that has the potential to enhance MXene's gas-sensing characteristics and has helped us get a deeper understanding of the sensing process between MXene and the target gas. To wrap things up, Pei et. al. [37]. examine the primary difficulties and potential of MXene-based materials in sensor applications. According to Guo et. al. [38].to present a highly sensitive Ti_3C_2Tx/WO3 composite resistive sensor for NH_3 detection. Selective NH_3 sensors based on polyaniline (PANI) nanofibers-supported Nb_2CTx nanosheets (Nb_2CTx/PANI) and directly driven by a simple triboelectric nanogenerator (TENG) are a promising approach to enhancing the responsiveness of NH_3 sensing [39]. For a self-powered supercapacitor and ammonia sensor using an electromagnetic-triboelectric hybrid generator, Wang and his colleagues [40]. describe in situ polymerization of polyaniline (PANI)/MXene (V_2C) composites. Authors Hosseini-Shokouh and his colleagues [36] using a combination of Ti_3C_2Tx flakes and conjugated polymers (poly[3,6-diamino- 10-methylacridinium chloride-3,6-diaminoacridine-squaraine] PDS-Cl) with polar charged nitrogen, the sensor performance was further optimized.

2. Properties of MXenes

2.1. Thermal Conductivity

The thermal conductivity of MXenes is a promising property for gas sensing. These 2D transition metal carbide and nitride nanomaterials are a class of materials that have unique thermal, electrical, and mechanical properties. They can be characterized by their composition and structure, which provides significant opportunities for designing new sensors with tunable thermal conductivity. MXenes can be produced from a variety of transition metal precursors. For example, Ti_3C_2Tx is a common MXene precursor, a good choice because it has high electrical conductivity and excellent thermal stability. Moreover, it is easy to produce and can be used as an effective sensor material because of its excellent gas-sensing performance. However, the MXenes derived from other MAX precursors such as graphite or carbon lampblack also have great potential for gas-sensing applications. The gas- sensing performance of MXenes is influenced by many factors, including their precursor material, defect density, flake size, and lateral dimensional. Therefore, a combination of these factors should be used to improve the gas-sensing performance of MXene-based sensors. Zha et. al., [40]. use first-principles simulations to study the electrical and thermal characteristics of semiconducting Sc_2CT_2 (T = F, OH) MXenes. The oxygen-functionalized M_2CO_2 (M = Ti, Zr, Hf) MXenes are studied for their thermal and electrical characteristics using first- principles calculations[41]. $Sc_3(CN)F_2$, in contrast to the metallic $Sc_3C_2F_2$ and $Sc_3N_2F_2$ has been shown to be a semiconductor with an indirect band gap of 1.18 eV [42]., thereby expanding the semiconducting family members of MXene. The authors of this piece are Sarikurt et. al. [43]. density functional theory and Boltzmann transport theory are used to determine the See beck coefficients and lattice thermal conductivity values of oxygen terminated M_2CO_2 (where M=Ti, Zr, Hf, Sc) monolayer MXene crystals with two different functionalization configurations (model-II (MD-II) and model-III (MD-III)). In spite of the fact that $Sc_3C_2F_2$ and $Sc_3N_2F_2$ are metallic, Luo et. al. [44], discover that $Sc3(CN)_2F_2$ is a semiconductor with an indirect band gap of 1.18 eV, thereby expanding the semiconducting family members of MXene.

In addition, the presence of fluorine functional groups at the surface of the MXenes may degrade their sensing performance. To maintain the sensitivity and selectivity of MXene- based gas sensors, strategies should be developed to control the ratio of fluorine in the synthesized MXenes. This can be achieved by using different etchants for the MAX phase and synthesis methods that preserve the surface-active sites. Furthermore, the synthesis of MXenes with large lateral dimensions and uniform terminations is another important factor to improve their gas-sensing performance. MXenes with a larger lateral dimension are able to better capture the gas molecules' surface energy, which can improve their sensitivity and selectivity. Using the first-principles calculations in conjunction with the quasi-harmonic approximation, Khaledialidusti and his colleagues [45]. explore the structural and mechanical characteristics of titanium-containing MXenes ($Tin^{+1}CnO_2$ (n = 1, 2)) as a function of temperature. Carbon fiber (CF)-MXenes foam was made using a straightforward freeze-drying technique; the CF was vertically oriented to create heat transfer pathways [46]. Titanium-containing MXenes ($Tin^{+1}CnO2$ (n = 1, 2)) are studied by Khaledialidusti et al[45]. who use first-principles calculations using a quasi-harmonic approximation to learn about their structural and mechanical characteristics as a function of temperature. Reference: Zhu and his colleagues [47]. It is possible to create a composite film with a thick and well-ordered layer-by-layer structure by first freeze-drying a three-dimensional foam, which improves the interfacial contact between neighboring MXene sheets and polyimide (PI) macromolecules, and then hot-pressing the foam. When the MXene sample is entirely dehydrated, the resistance-temperature relationship flips from negative to positive, as shown in the unique transient electrothermal tests presented by Yu and his colleagues [47].The polarity of the MXenes' surface-active sites can also affect their gas-sensing performance. For instance, MXenes containing hydroxyl and oxygen- terminated surfaces can better interact with polar inorganic gases and volatile organic compounds (VOCs). The interaction between the MXene and the polar molecules can cause an increase in the resistance of the MXene. The response of MXene-based sensors to VOCs and polar inorganic gases depends on the chemistry of the MXenes, which determines their conductivity. For example, MXene-derived titanium carbide has higher sensitivity to VOCs and polar inorganic gas molecules than carbon lampblack and graphite-based MXenes. This can be attributed to the higher metallic conductivity of the MXenes.

2.2 Electrical Properties

The sensitivity of MXenes depends on a number of factors, such as their surface electrical properties under different synthesis methods. Surface nearly free electron (NFE) states are an intriguing feature of several MXenes. These NFE states are close to the Fermi energy and provide nearly perfect transmission channels without nuclear scattering. This is beneficial for gas sensing because they are able to absorb large amounts of a target gas and transfer them to their surface. Xu and his colleagues [48].begin with a thorough first-principles calculation of the electron- phonon interactions to precisely determine the electron scattering rate, which they then employ to derive the optical and electrical characteristics of Ti_2AlC and two-dimensional MXenes, with no empirical parameters. Theragnostic for cancer, spintronics, and protecting against EMF contamination are only some of the electrical and magnetic property-based uses discussed in this article [49].

These properties of MXenes can be enhanced by modifying the surface functional groups, which influence their conductivity and ion transport. In particular, hydroxyl or oxygen- terminated MXenes have a high potential for

use in gas sensors because these terminations are hydrophilic and can easily bind ions. Moreover, in situ heating and biasing of MXenes has been shown to change their electronic properties in a way that can be beneficial for gas- sensing applications. By using unique transient electrothermal studies, Yu and his colleagues [48]. show that when the MXene sample is entirely dehydrated, the resistance-temperature relationship can flip from negative to positive. Rastin and his colleagues main goal is to prove that MXene cell-laden bioinks can be used for tissue engineering and that they can be used to 3D- print functional scaffolds for tissue regeneration. These results have provided new insights into the mechanisms affecting MXene conductivity and sensing properties, as well as a roadmap for future MXene-based sensors. Despite this, many MXene materials with mixed functional groups display metallic characteristics, as shown by a number of investigations [47]. So, conventional circumstances reveal conductivity in Ti_2C, V_2C, Nb_2C, and Ti_3C_2 as demonstrated by Ran and his colleagues [22]. The bandgap energy of a material is crucial for its use as a semiconductor. In **Table 2** we see that the bandgap energy of various MXenes ranges from 0.13 to 1.18 eV for transition metal disulfide/Sc_2CF_2 composites and from 0.24 to 1.0 eV for Ti_2CO_2, Zr_2CO_2, and Hf_2CO_2, respectively. Most conventional semiconductors can't function at temperatures lower than 100 °C when used for gas sensing. However, MXenes have been shown in certain research to be useful as NH_3 gas sensors at room temperature [48].

Table 2: Changes in the bandgap energy of MXenes with different functional groups [50].

S. No	Compound	Bandgap/eV
1	$Ti_3C_2(OH)_2$	**0.05**
2	$Ti_3C_2F_2$	0.10
3	Ti_2CO_2	1.03 Indirect bandgap
4	$Sc_2C(OH)_2$	0.45 Direct bandgap
5	Sc_2CF_2	1.80 Indirect bandgap
6	Sc_2CO_2	0.24 Indirect bandgap
7	Zr_2CO_2	0.88 Indirect bandgap
8	Hf_2CO_2	1.00 Indirect bandgap

When the MAX phase has the atomic layer A was removed, the MAX metal link was broken, and new atoms were bonded to the surface of the layer by covalent forces. Within each layer, atoms were confined to moving exclusively amongst themselves. As a result, electron mobility was greatly enhanced as atoms moved at high speeds in a small area. Sc_2CF_2 electron mobility anisotropy, for instance, was blatant even at ambient temperature. Sc_2CF_2 with a zigzag structure had an electron mobility of 5.03 X 10^3 cm^2 $v^{-1}s^{-1}$, which was about four times greater than that of Sc_2CF_2 with an armchair structure (1.07 X 10^3 cm^2 $v^{-1}s^{1}$)[56][51]. $Sc_2C(OH)_2$ had a more isotropic electron mobility. The overall electrical signal conversion in gas sensors is greatly enhanced by the exceptional electron migration characteristics of MXene materials.

2.3 Chemical Stability

The chemical stability of MXene-based gas sensors is one of the key aspects of their performance. The environmental instability caused by air, moisture, and light degrades MXenes in a short period of time, which can affect their sensitivity and selectivity. The oxidation of MXenes can also lead to severe degradation of their structural integrity, causing irreversible damage to their activity and performance. A variety of strategies and protective techniques can alleviate the oxidation of MXenes[52]. They include modifying the synthesis methods, defect passivation, dispersion medium, and storage conditions. Density Functional Theory (DFT) calculations based on a plane wave basis were used to study the reactivity and selectivity of four MXenes (i.e. M2C (M = Ti, V, Nb, Mo)) and their oxygen-functionalized forms (i.e. O-MXenes or M_2CO_2) toward gas molecules[53]. First-principles computations for the n = 1 structures of Sc, Ti, Zr, Mo, and Hf MXenes and their totally surface terminated forms with F and O are performed by Yorulmaz and his colleagues [54] . Additionally, morphology engineering can also provide MXenes with high capacity and long-term recycle stability without the use of co-catalysts or sacrificial reagents. Cheng and his colleagues [55]. report an approach to epitaxial growth of size-controlled noble nanometals on MXenes. When compared to conventional epoxy coatings, composites have far superior micropores and an impedance modulus that is 2 orders of magnitude greater. Zhao and his colleagues [56]. provide a reliable basis for the subsequent targeted regulation of the interaction between them.

Thermal annealing can significantly improve the thermal stability of MXenes. An unusual Ti3C2 nano bipyramid (Ti_2C_3NB) structure was formed via exfoliation, delamination, and hydrothermal treatment, as reported by Singh and his colleagues [57]. Heat treatment of MXenes can induce a range of crystal structure variations, including interlayer spacing reduction and defect healing. It also may induce a change in atomic structure, which could result in a twinning transformation and the formation of a new MXene phase, with improved intrinsic stability. Moreover, it has been shown that surface terminations can influence the oxidation stability of MXenes. For instance, synthesized MXenes with Cl^- terminations showed better thermal stability than F and =O terminated ones. Using $Ti_3C_2T_2$ (T = O, F, OH, and H) as an example of an MXene, Hu and his colleagues [58]. show that the termination stabilizes the Ti_3C_2 monolayer matrix by filling the nonbonding valence electrons of the surface Ti atom with the low-energy orbitals of the termination. New MAX phase alloy Mo_2ScAlC_2 with out-of-plane chemical order is predicted and experimentally confirmed by Meshkian and his colleagues [59] . It is therefore important to identify the effects of more and novel surface terminations on the stability of MXenes, which could provide new design rules for improving their thermal stability for various applications. Another technique that can help control the oxidation of MXenes is to etch or otherwise eliminate their surface functional groups (e.g., hydroxyls, sulfonates, amides, and methyl halides). The surface terminations of MXenes can affect their adsorption strength and selectivity toward specific gas species. For example, Ti_2CO_2 and Nb_2CO_2 adsorb NH_3 stronger than Mo_2CO_2 or V_2CO_2. In addition to these strategies, MXene-based sensors can be enhanced by incorporating other gas sensor components such as 2D nanomaterials, gold nanoparticles, nanotubes, metal oxides, polymers, and heterojunction interfaces. These materials are also known for their unique electronic properties and can improve MXenes' selectivity and sensitivity by interacting with the gas molecules at the heterojunction interfaces.

2.4 Mechanical Properties

The mechanical properties of 2D MXenes are a critical determining factor in gas sensor performance. The effectiveness of a MXene-based gas sensor depends on how well the material can withstand adsorption of the target molecules and resist changes in the sensitivity to gases. To achieve high performance, researchers must have a solid understanding of the relation between the materials properties and the structures of 2D MXenes. Several strategies and potential perspectives are available to improve the performance of MXene-based gas sensors, including the modulation of heterojunction interfaces, diverse stacking structures with controlled surface terminations, and combinations of MXenes with 2D nanomaterials, metal oxides, or polymers. These approaches have a significant potential to enhance gas- sensing sensitivity, but it is important to understand how they interact with the underlying mechanisms of MXene-based sensors and how to tailor their properties to suit different applications. Spray coating delaminated Ti_3C_2 MXene flakes is offered as a straightforward, scalable approach for fabricating transparent conductive thin films [60].Using 2D transition metal carbides (TMCs) as examples, we investigate the effects of a number of parameters on their mechanical characteristics (such as stiffness, flexibility, and strength) and electrochemical properties (such as ionic mobility, equilibrium voltage, and theoretical capacity) [61]. To this end Pang et. al., [62]. summarize the current advances in MXene research. $Ti_3C_2O_2$ with defects has an estimated modulus greater than graphene oxide's, making it the strongest 2D material yet to be produced by solution processing by Plummer and his colleagues [61]. Experiments with in-plane and cross-plane uniaxial compression of multilayer accordion-like MXene particles (Ti_2CTx and Ti_3C_2Tx) were reported by Li et. al., [63]. To begin, the degree to which MXenes react to polar organic molecules and oxidizing and reducing gases varies with the nature of the gas and the MXene Mechanical Properties. However, the problem of slow kinetics caused by the restacking of MXene nanosheets in electrodes is not well addressed, despite the fact that MXenes offer outstanding lithium storage performances due to their exceptional conductivity, excellent mechanical properties, and large interlayer spaces for ion intercalation. Using the mechanochemistry (MC) approach to induce strain in Ti3C2Tx MXene in order to optimize ion-transfer kinetics for lithium-ion batteries by Wang et. al., [64]. Graphene, hexagonal boron nitride (hBN), transition metal-dichalcogenides (MXenes), black phosphor, carbon nanomembranes (CNMs), 2D polymers, 2D metal organic frameworks (MOFs), and covalent organic frameworks are just some of the 2D materials that Zhang et. al. [65]. summarize recent progress in the mechanical characterization of (COFs).

3. Type of Gas sensor

Gas sensors rely on gas-sensitive materials for their operation. Modifications to the electrical resistance of gas-sensitive materials provide information about the gas's chemical make-up and concentration[66]. Different types of sensors exist based on their underlying technology, with semiconductor, catalytic combustion, electrochemical, optical, and thermal conductivity gas sensors all making the cut.

3.1 Gas sensors based on catalytic combustion technology

Components of catalytic combustion-type gas sensors are divided into two categories: measurement elements (also known as "black elements") and compensation elements (sometimes known as "white elements"). The component used for measurement is made up of a carrier and a catalyst. Wheatstone bridge theory lies at the heart of this circuit's operation. Balanced bridges have no voltage differential between their two arms[67]. As

the sensing gas and the circuit's sensitive element burn on the surface without an ignition source, the resistance of the measuring element rises. This causes a voltage differential across the bridge that is proportional to the gas concentration in the circuit. While these gas sensors are accurate, quick to respond, and reproducible, their application is restricted by the catalyst's short lifetime. To rectify the drawbacks of sphere-shaped sensors, a thick-film catalytic combustion hydrogen sensor [68].was created. The sensor is built on a ceramic sheet of alumina and uses a Wheatstone circuit bridge consisting of a hydrogen sensor and a compensating element to measure the gas's presence. What the sensor does is as follows: The resistance of the gas sensor rises as a result of heat produced when hydrogen interacts with air along the path of the measuring bridge arm. Thus, the bridge becomes unbalanced and an electrical current is produced. In order to determine the concentration difference of hydrogen, a voltage meter is used.

3.2 Electrochemical gas sensors

Electrochemical gas sensors are frequently employed for the detection of dangerous gases due to their high accuracy, fast response, and excellent selectivity. High-temperature, high- pressure, and high-concentration conditions are no match for sensors that can withstand them and enable autonomous measurement and control [69,70]. However, the production process grows more complex as more components are used. Diffusion filter membranes, an acid or alkali electrolyte tank, working electrodes, counter electrodes, and reference electrodes are the main components of electrochemical gas sensors [71]. The gas is removed from the air as it goes through the diffusive filter membrane and into the electrolyte, where it touches the working electrode to be oxidized and the counter electrode to be lowered in oxygen concentration. When the concentration of a detected gas is known, we may calculate its concentration by measuring the potential shift at the reference electrode [72]. The N2 experiment is essential for ensuring that the Pt electrodes' surfaces are properly exposed and ready for redox reactions. You can see the findings in **Fig. 4a**, which displays a typical CV curve for polycrystalline Pt in acidic medium [73]. All predicted electrochemical signals are present, confirming both the Pt surface quality and the Nafion ionic conductivity. The discovered signals are H adsorption/desorption situated between 0 and 0.25 V against SHE, the Pt oxide creation commencing at 0.7 V against SHE, the capacitive area plateau and the Pt oxides reduction peak at 0.7 V against SHE. Multiple sweep speeds ranging from 50 mV s1 to 200 mV s^{-1} are used in the experiment. It is typical for the current in electrochemical signals to rise as the sweep rate rises in cyclic voltammetry tests. Under the same circumstances, but with CO bubbling, we do a second electrochemical characterization. In **Fig. 4b**, we see the resultant curve. The basic form of the curve is comparable to that produced under N_2, but an oxidation peak emerges at 0.15 V versus MSE. This peak, when translated to the SHE scales [E(Pt) (CO_2/CO) ≃ 0.8 V against SHE] [74], represents the oxidation of CO into CO2 on the potential scale. This oxidation peak indicates that the sensor can detect CO by boosting the current at a voltage that corresponds to the gas's redox potential. This oxidation peak is present, and the current at the H ads/des peaks is slightly reduced as well. The fact that CO adsorbs to Pt at the same catalytic sites as H [75]. suggests that this process is indicative of the oxidation of CO into CO2. Yang and his colleagues [76]. prepared an ammonia-sensing material by alkalizing MXenes through the addition of NaOH to an aqueous Ti_3C_2Tx solution and consequently oxidizing the alkalized MXenes; the [O]/[F] ratio of the resultant material was three times that of the as-prepared MXenes. The abundant oxygen present on the surface of oxidized MXenes serves as a binding site for ammonia molecules. This prediction was supported by the high sensor response (28.87% at 100 ppm of

ammonia) in the presence of various concentrations of ammonia, as shown in **Figure 4c**. Similarly, Pazniak et .al. [77]. reported an ethanol sensor with partially thermally oxidized Ti3C2Tx. The oxidized MXene-based gas sensor showed a faster response time and 45-times higher response at 250 ppm of ethanol than the as-prepared MXene sensor. Furthermore, in addition to TiO2 NWs, silver NPs (AgNPs) also facilitate charge conduction and thus, improve the capacitive response of the sensors [78]. The sensing mechanism here can be explained as follows. As humidity increases, the number of water molecules adsorbed on the active sites of the MXene nanosheets (MNSs) electrode increases. Each adsorbed water molecule is then ionized to a hydronium ion under an external electric field, and the capacitance gradually increases because of increased ion conductivity. The added AgNPs contribute to enhancing the sensitivity by 106 800% via promoting water adsorption and lowering the activation energy of water molecules and MXene film. The humidity sensor based on this sensing mechanism showed a fast response, good reliability in various relative humidity (RH) environments (**Fig.4d**) and outperformed previously reported humidity sensors (**Fig.4 e**). Liu and his colleagues [79]. promoted the adsorption of water molecules on the MXene electrode surface by enhancing its hydrophilicity through plasma treatment. The success of this strategy suggests that the performance of capacitance-type MXene sensors can be improved by introducing a secondary material and various other post-treatment methods. Desai et al. [80]. fabricated a sensor for Ag and Mn ions using MNSs. The MNSs were obtained by the addition of tetramethylammonium hydroxide (TMAOH) to Ti_3C_2 MXene solution and subsequent fragmentation via ultrasonication, as shown in **Fig 4f**. The synthesized MNSs absorbed 381 nm UV light and showed a PL emission peak at 461 nm via the quantum confinement effect. After the researchers examined the fundamental PL characteristics of the MNSs, they investigated the sensing performance toward various ions. Among the examined ions, Ag ions and Mn ions caused strong PL quenching (**Fig 4g**), which resulted in LOD values of 9.7×10^{-9} m and $0.10^2 \times 10^{-6}$ m, respectively. In addition to the aforementioned PL measurement, light measurement can be used as the basis for various strategies, e.g., Nano plasmonic colorimetric sensing[81].

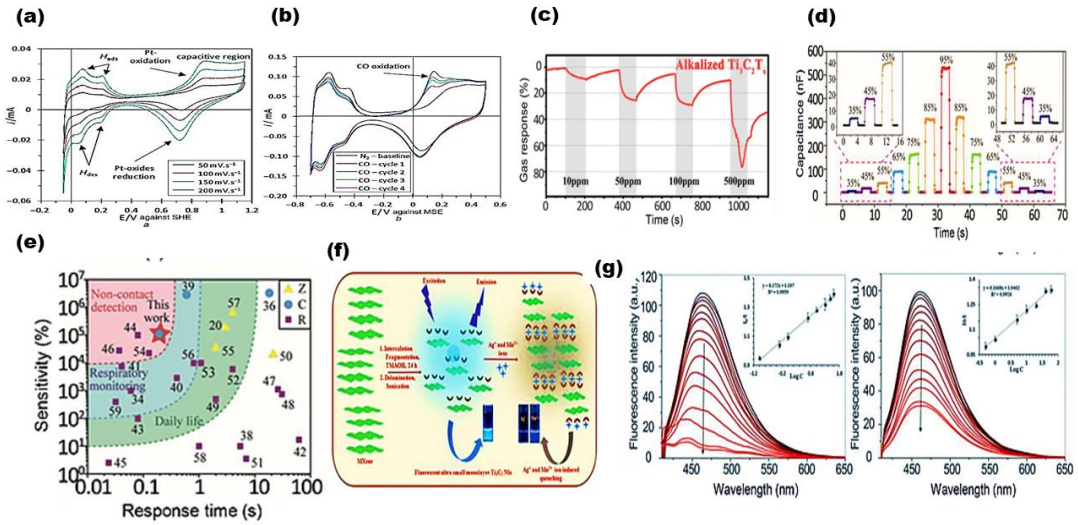

Figure 4: Electrochemical characterization (a) Three-electrode cyclic voltammetry with varying sweep speeds in H2SO4 0.1 mol l^{-1};(b) Cyclic voltammetry at 200 mV s1 in H_2SO_4 0.1 mol^{-1} with various gases bubbling in

the cell; all normal signals from polycrystalline Pt in acidic media are present; signal rises with sweep rate. When CO is converted to CO_2, a signal occurs right before the capacitive zone of Pt oxides; (c) Response of device based on alkalized Ti_3C_2Tx to different RH environments [82];(d) Response and recovery characteristics of sensor TA_2 exposed to different RH environments [83]; (e) Comparison of responses, recovery times, and sensitivities of sensor TA_2 fabricated by Li and his colleagues with those of other humidity sensors reported in the literature; the red region represents the requirements of a touchless interface for response speed and sensitivity of humidity sensor[83]; f) Schematic representation of preparation of fluorescent ultrasmall Ti_3C_2 nanosheets and their application to sensitive and selective fluorescence detection of Ag^+ and Mn^{2+} ions[84]. g) Fluorescence emission spectra of Ti_3C_2 nanosheets with various concentrations of (left) Ag^+ ions (0.1–100 × 10-6 m) and (right) Mn^{2+} (0.5–500 × 10-6 m). The inset plots show the linear relationships between the fluorescence intensity of the Ti_3C_2 nanosheets and the different concentrations of Ag^+ ions (linear range of graph: 0.1–40 × 10-6 m) and Mn^{2+} ions (linear range of graph: 0.5–60 × 10-6 m); here, I0 and I denote, respectively, the fluorescence intensities of the Ti_3C_2 nanosheets at 461 nm in the absence and presence of Ag^+ and Mn^{2+} ions[84].

3.3 Thermal conductivity gas sensors

The thermal conductivity of the gas being measured provides the basis for the operation of thermal conductivity gas sensors. A portion of the thermistor's heat, generated by the current within the instrument, is dissipated when the gas passes through the detecting unit, resulting in a change in resistance. You may utilize the heat conduction to figure out the gas concentration, which varies with different gases and gas concentrations [40]. Despite its low precision and huge mistakes, such sensors have a number of benefits, including a wide detection range, reasonable stability, a simple construction, low cost, and reduced consumption. Among the gas sensors presented in this part, semiconductor gas sensitive sensors offer apparent benefits in terms of production cost, responsiveness, and sensitivity. A lot of people are interested in using MXenes as physical sensors because of its great electrical conductivity and water dispersibility. Previous work has shown that certain MXene-based physical sensors can detect a variety of human movements; as a result, there is hope that these sensors may find practical use in areas like healthcare monitoring. Research on physical sensors based on MXene has therefore intensified, with the goal of making them more practical and enhancing their performance. Strain, pressure, temperature, and photosensors are the four main types of physical sensors based on MXene [85]. Researchers mostly focus on strain and pressure sensors when studying MXene-based physical sensors due to the piezoresistive characteristic shown by MXene-based composites or MXenes. Stacks of MXene flakes exhibit piezoresistive properties via the following process. The sensor's ability to detect strain depends on the stability of the connections between the MXene flakes that are dispersed throughout the surface of the low Young's modulus polymer. Because of this, MXene becomes susceptible to stress or pressure from outside sources, since its electrical resistance changes. Thus, the macroscopic structure and dimensions of the sensing platform depend on the piezoresistive properties of the strain and physical sensors. For this reason, there are three subtypes of strain and pressure sensors based on MXene: 1D fibrous, 2D thin-film, and 3D-structured. This categorization according to the size of the sensor's components is significant since it sheds light on how to improve the sensing capability. Check out **Table 3** for some examples of performance metrics used to measure strain and pressure sensors. These include pressure sensitivity, sensing range, detection limit, reaction time, and gauge factor (GF).

Most importantly, a sensor with a high sensitivity and GF may detect weak-intensity stimuli satisfactorily. These parameters are defined as the linear slope of the electrical output as a function of strain or pressure. Consequently, the next section assesses the performance of strain and pressure sensors based on MXene using these two critical characteristics.

Table 3: for some examples of performance metrics used to measure strain and pressure sensors.

Probing method	**Year**	**MXene species**	**Target**	**Limit of detection**	**Response time**	**Sensitivity**	**Working range**	**Refs.**
Piezoresistive	2020	$Ti_3C_2T_x$	Strain	N/A	N/A	12 900 (multiregional)	0%–175% (single), 0%–200% (yarn)	[86]
Capacitive	2020	$Ti_3C_2T_x$	Pressure	1.5 Pa (empirical)	N/A	0.51 kPa^{-1} (<1 kPa), 0.01 kPa^{-1} (10–100 kPa)	0–100 kPa	[88]
Piezoresistive	2019	$Ti_3C_2T_x$	Strain	N/A	344 ms	128 (<15%), 800 (15%–25%), 1553 (25%–50%), 3.2 x 10^5 (50%–70%), 3 x 10^6 (70%–85%), 1.6 x 10^7 (85%–100%)	0%–100%	[87]
Piezoresistive	2019	$Ti_3C_2T_x$	Strain	N/A	N/A	309.10 (□60%), 474.38 (60%–150(150%–200%)%), 872.79	0%–200%	[88]
Piezoresistive	2018	$Ti_3C_2T_x$	Strain	N/A	N/A	11.5 (<35%)	0%–40% (tensile), r < 2.5 mm (bending)	[89]
Piezoresistive	2019	$Ti_3C_2T_x$	Strain	0.00025 (empirical)	300 ms	190.8 (<52.6%), 1148.2 (52.6%–74.1%)	0%–74.1%	[90]
Piezoresistive	2018	$Ti_3C_2T_x$	Strain	0.001 (empirical)	6000 ms	2 (<5%), 64.6 (0%–30%), 772.6 (40%–70%)	0%–70%	[91]
Piezoresistive	2019	$Ti_3C_2T_x$	Pressure	24.5 Pa (empirical)	N/A	182.85 kPa^{-1} (<735 Pa), 516.74 kPa^{-1} (735–2205 Pa)	24.5–2205 Pa	[[92]
Piezoresistive	2019	$Ti_3C_2T_x$	Strain	0.00025 (empirical)	140 ms	178.4	0%–53%	[93]
Piezoresistive	2020	$Ti_3C_2T_x$	Strain	N/A	N/A	3.18	0.86%–2.09% (bending)	[94]
Piezoresistive	2019	$Ti_3C_2T_x$	Pressure	10.2 Pa (empirical)	11 ms (response), 25 ms (recovery)	0.55 kPa^{-1} (0.023–0.982 kPa), 3.81 kPa^{-1} (0.982–10 kPa), 2.52 kPa^{-1} (10–30 kPa)	0–30 kPa	[89, 95]
Piezoresistive	2019	$Ti_3C_2T_x$	Pressure	N/A	26 ms (response),	3.844 kPa^{-1} (<29 kPa), 12.095 kPa^{-1} (29–40 kPa)	0–40 kPa	[96]
					50 ms (recovery)			
Piezoresistive	2020	$Ti_3C_2T_x$	Pressure	0.005 N (empirical)	N/A	N/A	0.005–0.6 N	[97]
Piezoresistive	2020	$Ti_3C_2T_x$	Pressure	9 Pa (empirical)	4 ms	99.5 kPa^{-1}	0–4.5 kPa	[98]
Piezoresistive	2020	$Ti_3C_2T_x$	Pressure	13 Pa (empirical)	50 ms (response),	11.47 kPa^{-1} (0.013–0.77 kPa), 0.23 kPa (2–10 kPa)	0–10 kPa	[99]

					20 ms (recovery)			
Piezoresistive	2019	$Ti_3C_2T_x$	Strain	N/A	N/A	256.1 (<5%), 433.3 (15%–35%), 1160.8 (35%–60%),	0%–83%	[100]
						2209.1 (60%–77%), 8767.4 (77%–83%)		
Piezoresistive	2019	$Ti_3C_2T_x$	Pressure	8 Pa (empirical)	14 ms (response),	24.63 kPa^{-1} (<0.2 kPa), 1.18 kPa^{-1} (0.2–7 kPa)	7 kPa	[101]
					216 ms (recovery)			
Piezoresistive	2020	$Ti_3C_2T_x$	Pressure	4.4 Pa (empirical)	130 ms (response),	151.4 kPa^{-1} (<4.7 kPa), 33.8 kPa^{-1} (4.7–15 kPa)	0–15 kPa	[102]
					104 ms (recovery)			
Piezoresistive	2020	Ti_2CT_x	Pressure	8 Pa (empirical)	60 ms (response), 40 ms (recovery)	507 kPa^{-1} (<5.75 kPa), 225 kPa^{-1} (5.75–12 kPa), 25 kPa^{-1} (12–40 kPa)	0–40 kPa	[103]
Piezoresistive	2020	$Ti_3C_2T_x$	Pressure	N/A	N/A	N/A	N/A	[104]
Piezoresistive	2020	$Ti_3C_2T_x$	Pressure	89 kPa (empirical)	1 s (response), 5 s(recovery)	0.00232 kPa^{-1}	126–168 kPa	[107]
Piezoresistive	2020	$Ti_3C_2T_x$	Strain	0.001 (empirical)	50 ms	107.43 (<10%)	0%–75%	[105]
Piezoresistive/(capacitive)	2019	$Ti_3C_2T_x$	Strain	N/A	165 ms, 190 ms	1.2 (resistive), 0.4 (capacitive)	0%–400% (resistive), 0%–200%(capacitive)	[106]

3.4 MXene-based gas sensors

Due to their excellent metal conductivity, robust ion-transmission capabilities, biocompatibility, broad specific surface area, and simple surface functionalization potential, MXenes are appealing materials in the sensor industry [37] .**(Table 4).** However, there is a dearth of information on how MXenes may be used as gas detectors. Composite gas-sensitive materials with great performance, which often include MXene components, are the most common use of this technology for sensing gases. The ability of these systems to hold gas molecules is facilitated by the presence of voids in the MXenes' intermediate layer [107]. In addition to their usefulness as gas sensors, MXenes have the added benefits of great selectivity due to the presence of surface functional groups and excellent stability, both of which are essential in the harsh industrial conditions in which they will be used. Sc2C, the MXene with the highest theoretical specific surface area per unit weight, has the potential to dramatically increase the sensitivity of a gas sensor since it can operate via three adsorption

mechanisms: chemical adsorption, Kubas adsorption, and physical adsorption [108]. Varying gases have different adsorption energies at the MXene surface, as shown in **Fig. 5a [109]**.

Table 4: Gas sensitivity data of MXene-based composite materials for different gases.

Core material	**Object gas**	**Operation temperature(°C)**	**Response time**	**Gas response (R g/Ra)**	**Ref.**
Ti_3C_2TX	Acetone	RT	NA	0.125/200ppm	[16]
$W_{18}O_{49}/Ti_3C_2X$	Acetone	300	4.6s/20ppm	11.6/20ppm	[79]
CuO/Ti_3C_2TX MXene	Toluene	250	270s/50ppm	11.4/50ppm	[80]
$MXene/SnO_2$	NH_3	RT	36s/50ppm	40/50ppm	[81]
$MXene/TiO_2$	NH_3	RT	60s/10ppm	3.1/10ppm	[81]
$Li\text{-}V_2CTX$	NH_3	RT	41s/50ppm	3.41/500ppm	[81]
$HF\text{-}V_2CTX$	methane	RT	169s/500ppm	1.49/500ppm	[81]
$Cl\text{-}Ti_3C_2TX$	NH_3	RT	98s/500ppm	13.2/500ppm	[81]
Co_3O_4@PEI/Ti_3C_2Tx	NO_X	RT	27.9s/30ppb	N/A	[110]
$MXene/Co_3O_4$	HCHO	RT	83s/10ppm	9.2/10ppm	[40]
SnO-SnO_2/Ti_3C_2TX	Acetone	RT	18s/100ppm	12.1/100ppm	[89]
$Ni(OH)2/Ti_3C_2Tx$	NH_3	RT	78s/50ppm	6.2/10ppm	[111]

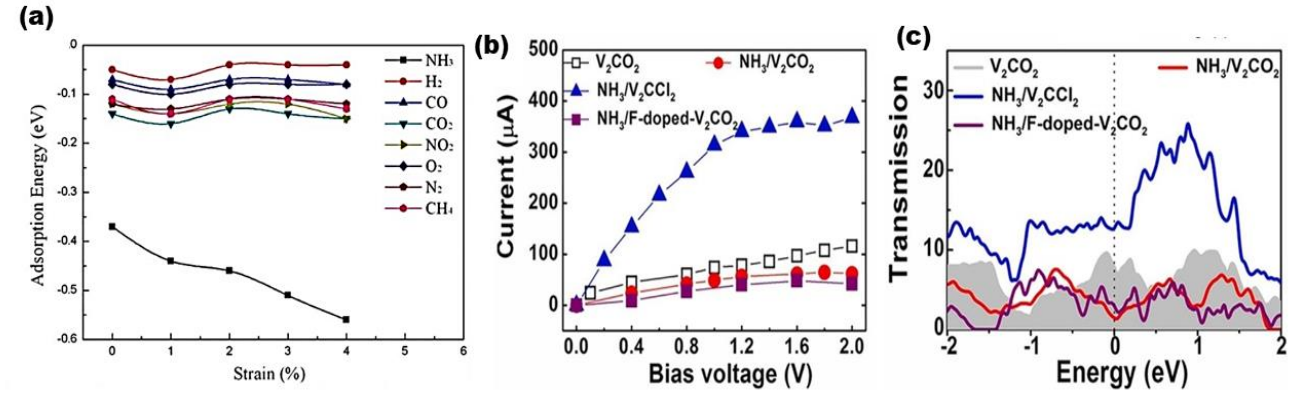

Figure 5: (a)Adsorption energies of different gases at the Ti_2CO_2 MXene surface [112]. (b) I-V curves along the ZZ direction. (c) Corresponding transmission spectra under 0V bias for V2CO2- based systems, respectively. The Fermi energy was shifted to zero [113].

3.5 NH_3 gas sensors

Toxic and dangerous ammonia (NH_3) gas is also very flammable. Wastewater and waste gas containing NH_3 are being released into the environment due to the growth of the chemical industry, posing a risk to human health and aquatic life. Consequently, research on gas sensors for precise NH3 detection is crucial. The chemical adsorption of NH_3 on single-layer Ti_2CO_2 generates a charge transfer of 0.174 Ev [109] suggesting and significant alterations in the electron transmission function and IV single bond properties, and resulting in the material's great sensitivity and selectivity for NH_3. Because NH3 adsorption may be reversed, single- layer Ti_2CO_2 material may be useful as a sensor for NH_3.

When studying the interaction between NH and O-terminal MXenes with various charges (M_2CO_2, M = Sc, Ti, Zr, and Hf), Xiao and his colleagues [114]. found that NH_3 molecules were considerably adsorbed on M_2CO_2 with evident electron transfer. Controlling the electron injection also made NH3 release simple, indicating that these MXenes may be useful as reusable NH_3 sensor materials. To analyze human breath for an accurate health diagnosis, Sinha and his colleagues (2018) constructed a wearable sensor employing an MXene material that can efficiently detect NH_3, ethanol, and acetone[115]. Patients with diabetes often exhale acetone gas, while those with lung disorders often exhale NH3. When tested with low concentrations of acetone (11.6-20 ppm), the $W_{18}O_{49}/Ti_3C_2Tx$ composite materials that Sun and his colleagues [116] produced showed a quick reaction speed in addition to high selectivity and stability. By using a solvothermal technique, the same team was able to eliminate the fluorine-containing groups from the MXene material, improving its surface chemical characteristics and opening up novel avenues for the research and development of acetone hybrid materials. Schematic of the detecting process of NH_3 sensors is shown in **Fig. 5b**. The gas-sensitive features of V_2CTx MXene were studied theoretically by analyzing the transport properties of monolayer V_2CTx with DFT calculations and a two-probe device model to depict the change in conductivity [117]. Layers of V_2CO_2

Monolayers (assuming "O" dominates the functional groups) **Fig. 5d** shows the I V curves before and after NH3 adsorption, and the current value via the sensor was around three times higher in the zigzag direction than in the armchair direction. As illustrated in **Fig. 5f**, this procedure led to a decrease in conductivity, which may be explained by the smaller number of conductance channels available for electron transport towards the Fermi level. After NH3 adsorption, V_2CF_2 (given that "F" dominates the functional groups) showed poorer conductivity and a bigger positive response compared to its unmodified state. Furthermore, as can be shown in **Fig. 5e**, the V_2CC_{l2} (given that "Cl" dominates the functional groups) demonstrated a higher current through the sensor following NH3 adsorption. This means that gas sensors based on V_2CT_x can flip from a positive to a negative response when the single bond Cl functional group is present.

3.6 NOx gas sensors

As people become more conscious of the need to preserve the natural world, they also become more concerned about the state of the air they breathe. There is a critical need for advanced monitoring equipment that can detect NOX and other important air contaminants. Together with hemoglobin, NOx can irritate the lungs and lead to a wide range of illnesses[118]. That's why it's crucial to keep an eye on the relative amounts of different gases in indoor spaces like homes and offices. Musing ultrasonic spray pyrolysis technology, Yang and his colleagues [119]. prepared a 3D-shrinkage MXene nanosphere/ZnO composite sensitive electrode to address problems such as the simple stacking of 2D MXene Ti3C=TX nanofilms and the subsequent loss of their high specific surface area, which had become the limiting factor in further improvements to the electrode's performance **(Fig. 6a).** Self-assembly led to the formation of a 3D crumpled MXene sphere/ZnO composite, which began as MXene flakes coated with ZnO nanoparticles. The 3D crumpled MXene sphere has a uniform coating of ZnO nanoparticles, as seen in the TEM photos **(Fig. 6b)**. At the same time, the composite-material sensor showed high selectivity and sensitivity to NO2 gas **(Fig. 6 c-e).** Koh and his colleagues [120]. investigated how gas-induced swelling of Ti3C2TX MXene films affected their sensitivity to gases. The results show that the gas-sensing channel treated with 0.3 mM NaOH exhibited the highest swelling capacity and highest selectivity to ethanol vapor. They showed that interlayer movement in MXenes must be regulated.

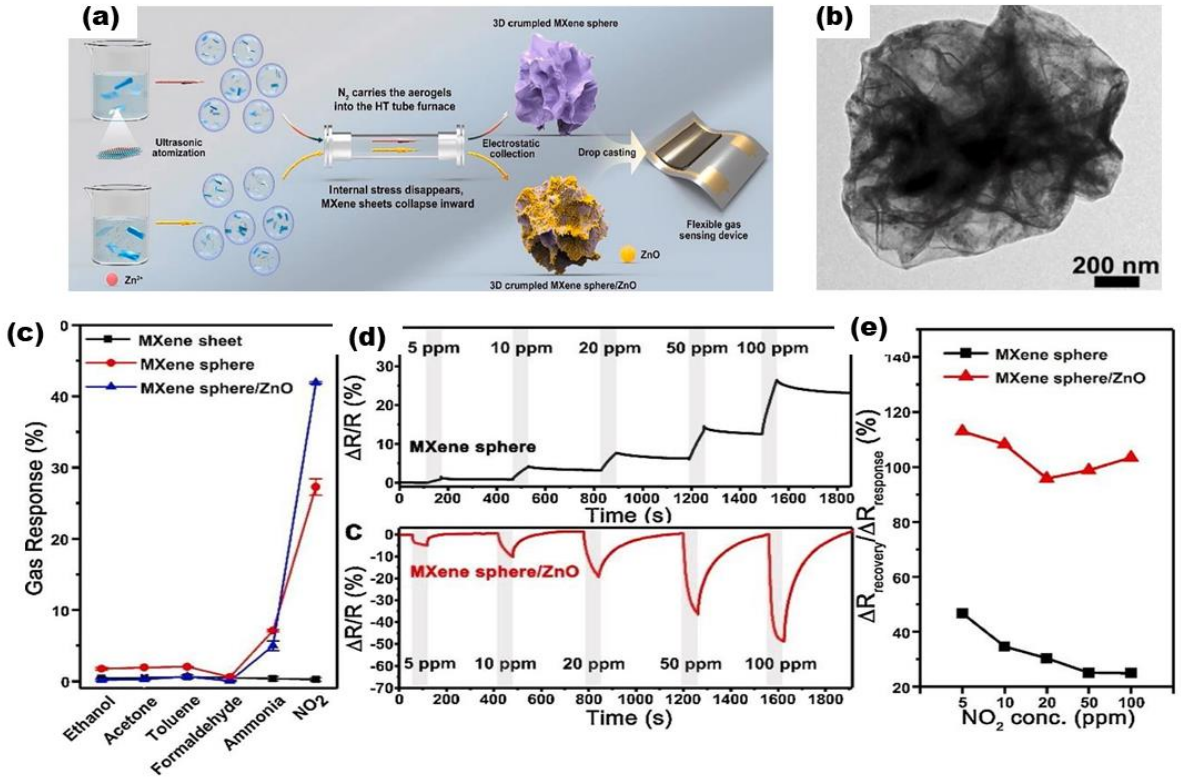

Figure 6: (a) A simplified diagram showing the steps involved in making a flexible gas sensing device and 3D-crumpled MXene spheres;(b) 3D crumpled MXene sphere/ZnO morphology and element distribution; Comparison of MXene sheet, 3D crumpled MXene sphere, and 3D crumpled MXene sphere/ZnO based flexible gas sensors for selectivity, concentration sensitivity, and recovery. (c) The sensitivity to different target gases at a concentration of 100 ppm of MXene sheet, MXene sphere, and MXene sphere/ZnO based sensors. (d-e) Relative humidity (RH) at 70% and concentrations of NO2 (5, 10, 20, 50, and 100 ppm) measured using MXene sphere and MXene sphere/ZnO sensors. Sensors based on MXene spheres and MXene sphere/ZnO to various concentrations of NO2 (d) The recovery rate (Recovery/Response) [39].

4. Conclusions and outlook

MXenes are a novel family of two-dimensional materials with remarkable properties that have attracted a lot of attention due to their high value in a wide range of industries. Due to the distinctive 2D structure of MXenes, which allows for tunable surface-mediated characteristics and an intrinsically large specific surface area, MXene-based sensors have been extensively studied. Researchers have been looking at ways to increase the sensitivity and selectivity of chemical, biological, and physical sensors using MXene-based sensors. These methods include surface functionalization, macro structuring, and composite creation. One of the most encouraging findings from these sensors' study is that the surface modification of MXene does not compromise the outstanding electrical conductivity inherent to pure MXenes. For instance, without sacrificing conductivity, it is conceivable to raise the analyte adsorption energy on the MXene surface. Research into enhancing sensor

performance through the use of the aforementioned methods has generally shown positive results**.** As a whole, researchers in this area are currently concentrating on finding out how well MXenes can transfer their useful properties to sensors, namely in the areas of sensitivity. In order to bring sensors based on MXene to market, several elements are essential. Some practical features, such as MXenes' stability, multifunctionality, and productivity, need to be addressed before they can be employed successfully in the industry.

- **Reliability and stability:** In contrast to other conductive low-dimensional nanomaterials like graphene, AgNWs, and CNTs, MXenes experiences intense oxidation when exposed to room temperature. Hence, more study into making MXenes more stable is needed so that they can last the environment and, in turn, make MXene-based sensor systems more reliable in terms of performance.
- **Efficiency**: The fabrication procedures that have been discussed so far for using MXenes as sensing materials do not meet the current industrial standards in terms of throughput and yield. The development of trustworthy and scalable fabrication procedures that are appropriate for mass production should be the focus of future research in order to circumvent this challenge without compromising sensor performance.
- The **versatility** of MXenes as a sensing material shows that it might replace traditional materials that can only detect one analyte or stimulus at a time, thanks to its multifunctionality and multimodal application. From a commercialization perspective, however, existing research has not adequately addressed these MXene features; this area of study might produce a simple high-throughput sensor technology applicable to real-world complicated multicomponent systems. Therefore, MXenes' multifunctionality should be the center of future study.

Among the many possible applications of MXene, a groundbreaking 2D layered crystal with an unusual structure and a high surface area, are energy storage, catalysis, and gas sensitivity. Still, MXene compounds should not be prepared using the HF etching process because of the risks involved. Using HCl/LiF mixtures instead of HF can reduce experiment safety, but the quality of the resulting MXenes is poor. There have been considerable advancements in the creation of high-efficiency gas sensors using MXene materials with enhanced semiconductor performance, while this field is still in its early stages. This innovative 2D crystal material shows promise as a gas sensor, but further study is required to confirm this.

Acknowledgements

Authors acknowledge the Dr. Vandana, IUAC, New Delhi for the help during the work.

5. Conflict of interest

Authors have no conflict of interest with any work.

References

[1]. Li, Q., Y. Li, and W.J.C. Zeng, Preparation and application of 2D MXene-based gas sensors: A review. 2021. **9**(8): p. 225.

[2]. Hasan, M.M., M.M. Hossain, and H.K.J.J.o.M.C.A. Chowdhury, Two-dimensional MXene-based

flexible nanostructures for functional nanodevices: a review. 2021. **9**(6): p. 3231-3269.

[3]. Shahzad, F., et al., 2D transition metal carbides (MXenes): applications as an electrically conducting material. 2020. **32**(51): p. 2002159.

[4]. Xin, M., et al., MXenes and their applications in wearable sensors. 2020. **8**: p. 297.

[5]. Alwarappan, S., et al., 2D metal carbides and nitrides (MXenes) for sensors and biosensors. 2022. **205**: p. 113943.

[6]. Di Tinno, A., et al., Sensitive detection of industrial pollutants using modified electrochemical platforms. 2022. **12**(10): p. 1779.

[7]. Cancelliere, R., et al., Biochar: a sustainable alternative in the development of electrochemical printed platforms. 2022. **10**(8): p. 344.

[8]. Zhang, H.-F., et al., Strategies and challenges for enhancing performance of MXene-based gas sensors: a review. 2022. **41**(12): p. 3976-3999.

[9]. Xu, W., et al., The metallic nature of two-dimensional transition-metal dichalcogenides and MXenes. 2021. **76**(4): p. 100542.

[10]. Kumar, S.J.S., Fluorine-Free MXenes: Recent Advances, Synthesis Strategies, and Mechanisms. 2024. **20**(16): p. 2308225.

[11]. Zhang, Y.Z., et al., MXene printing and patterned coating for device applications. 2020. **32**(21): p. 1908486.

[12]. Zheng, W., et al., Heterolayered SnO2/SnSe nanosheets for detection of NO2 at room temperature. 2022. **5**(2): p. 2436-2444.

[13]. Ahmed, B., et al., H 2 O 2 assisted room temperature oxidation of Ti 2 C MXene for Li-ion battery anodes. 2016. **8**(14): p. 7580-7587.

[14]. Naguib, M., et al., Two-dimensional nanocrystals produced by exfoliation of Ti3AlC2, in MXenes. 2011, Jenny Stanford Publishing. p. 15-29.

[15]. Kumar, S., et al., Effect of Ti 3 C 2 T x MXenes etched at elevated temperatures using concentrated acid on binder-free supercapacitors. 2020. **10**(68): p. 41837-41845.

[16]. Zhang, X., et al., A review on optoelectronic device applications of 2D transition metal carbides and nitrides. 2021. **200**: p. 109452.

[17]. He, T., et al., MXene/SnO2 heterojunction based chemical gas sensors. 2021. **329**: p. 129275.

[18]. Lee, E., et al., Room temperature gas sensing of two-dimensional titanium carbide (MXene). 2017. **9**(42): p. 37184-37190.

[19]. Anasori, B. and Û.G. Gogotsi, 2D metal carbides and nitrides (MXenes). Vol. 2549. 2019: Springer.

[20]. Peng, C., et al., A hydrothermal etching route to synthesis of 2D MXene (Ti3C2, Nb2C): Enhanced exfoliation and improved adsorption performance. 2018. **44**(15): p. 18886-18893.

[21]. Ran, J., et al., Ti3C2 MXene co-catalyst on metal sulfide photo-absorbers for enhanced visible-light photocatalytic hydrogen production. 2017. **8**(1): p. 13907.

[22]. Al-Dulaimi, N., et al., Sequential bottom-up and top-down processing for the synthesis of transition metal dichalcogenide nanosheets: the case of rhenium disulfide (ReS 2). 2016. **52**(50): p. 7878-7881.

[23]. Zang, X., et al., Enhancing capacitance performance of Ti 3 C 2 T x MXene as electrode materials of supercapacitor: from controlled preparation to composite structure construction. 2020. **12**: p. 1-24.

[24]. He, Z., et al., Two-dimensional TiVC solid-solution MXene as surface-enhanced Raman scattering substrate. 2022. **16**(3): p. 4072-4083.

[25]. Feng, W., et al., Ultrasonic assisted etching and delaminating of Ti3C2 Mxene. 2018. **44**(6): p. 7084-7087.

[26]. Le, T.A., et al., Porosity-engineering of MXene as a support material for a highly efficient electrocatalyst toward overall water splitting. 2020. **13**(5): p. 945-955.

[27]. Natu, V., et al., 2D Ti3C2Tz MXene synthesized by water-free etching of Ti3AlC2 in polar organic solvents. 2020. **6**(3): p. 616-630.

[28]. Fatima, M., et al., Experimental and computational analysis of MnO2@ V2C-MXene for enhanced energy storage. 2021. **11**(7): p. 1707.

[29]. Zhang, T., et al., Synthesis of two-dimensional Ti3C2Tx MXene using HCl+ LiF etchant: enhanced exfoliation and delamination. 2017. **695**: p. 818-826.

[30]. Wu, Y., et al., Few-layer MXenes delaminated via high-energy mechanical milling for enhanced sodium-ion batteries performance. 2017. **9**(45): p. 39610-39617.

[31]. Wang, Z., et al., Facile fabrication of flexible rGO/MXene hybrid fiber-like electrode with high volumetric capacitance. 2020. **448**: p. 227398.

[32]. Zhao, W.-N., et al., A high-performance trace level acetone sensor using an indispensable V 4 C 3 T x MXene. 2020. **10**(3): p. 1261-1270.

[33]. Dong, X., et al. A Novel Memory Mechanism for Postponing the Drift of Chemical Gas Sensors. in 2021 IEEE 11th International Conference on Electronics Information and Emergency Communication (ICEIEC) 2021 IEEE 11th International Conference on Electronics Information and Emergency Communication (ICEIEC). 2021. IEEE.

[34]. Sun, B., et al., Co 3 O 4@ PEI/Ti 3 C 2 T x MXene nanocomposites for a highly sensitive NO x gas sensor with a low detection limit. 2021. **9**(10): p. 6335-6344.

[35]. Naguib, M., et al., Two-dimensional transition metal carbides. 2012. **6**(2): p. 1322-1331.

[36]. Chen, W.Y., et al., Surface functionalization of Ti3C2T x MXene with highly reliable superhydrophobic protection for volatile organic compounds sensing. 2020. **14**(9): p. 11490-11501.

[37]. Pei, Y., et al., Ti3C2TX MXene for sensing applications: recent progress, design principles, and future perspectives. 2021. **15**(3): p. 3996-4017.

[38]. Guo, L., et al., Extremely high thermal conductivity of carbon fiber/epoxy with synergistic effect of MXenes by freeze-drying. 2020. **19**: p. 134-141.

[39]. Yang, Z., et al., Flexible resistive NO2 gas sensor of three-dimensional crumpled MXene Ti3C2Tx/ZnO spheres for room temperature application. 2021. **326**: p. 128828.

[40]. Wang, S., et al., PANI nanofibers-supported Nb2CTx nanosheets-enabled selective NH3 detection driven by TENG at room temperature. 2021. **327**: p. 128923.

[41]. Wang, X., et al., In situ polymerized polyaniline/MXene (V2C) as building blocks of supercapacitor and ammonia sensor self-powered by electromagnetic-triboelectric hybrid generator. 2021. **88**: p. 106242.

[42]. Hosseini-Shokouh, S.H., et al., Highly Selective H2S Gas Sensor Based on Ti3C2T x MXene–Organic Composites. 2023. **15**(5): p. 7063-7073.

[43]. Sarikurt, S., et al., The influence of surface functionalization on thermal transport and thermoelectric properties of MXene monolayers. 2018. **10**(18): p. 8859-8868.

[44]. Liu, J., et al., H2S detection sensing characteristic of CuO/SnO2 sensor. 2003. **3**(5): p. 110-118.

[45]. Khaledialidusti, R., A.K. Mishra, and A.J.J.o.M.C.C. Barnoush, Atomic defects in monolayer ordered double transition metal carbide (Mo 2 TiC 2 T x) MXene and CO 2 adsorption. 2020. **8**(14): p. 4771-4779.

[46]. Elemike, E.E., et al., The future of energy materials: A case of MXenes-carbon dots nanocomposites. 2022. **50**: p. 104711.

[47]. Yu, Z., et al., Fabrication of ZnO/Carbon quantum dots composite sensor for detecting NO gas. 2020. **20**(17): p. 4961.

[48]. Li, X., et al., Intriguing electronic properties of two-dimensional MoS2/TM2CO2 (TM= Ti, Zr, or Hf) hetero-bilayers: type-II semiconductors with tunable band gaps. 2015. **26**(13): p. 135703.

[49]. Khaledialidusti, R., B. Anasori, and A.J.P.C.C.P. Barnoush, Temperature-dependent mechanical properties of Ti n+ 1 C n O 2 (n= 1, 2) MXene monolayers: A first-principles study. 2020. **22**(6): p. 3414-3424.

[50]. He, T., et al., Endohedral metallofullerenes (M@ C60) as efficient catalysts for highly active hydrogen evolution reaction. 2017. **354**: p. 231-235.

[51]. Sinha, A., et al., MXene: An emerging material for sensing and biosensing. 2018. **105**: p. 424-435.

[52]. Cao, F., et al., Recent advances in oxidation stable chemistry of 2D MXenes. 2022. **34**(13): p. 2107554.

[53]. Shein, I. and A.J.C.M.S. Ivanovskii, Graphene-like titanium carbides and nitrides Tin+ 1Cn, Tin+ 1Nn (n= 1, 2, and 3) from de-intercalated MAX phases: First-principles probing of their structural, electronic properties and relative stability. 2012. **65**: p. 104-114.

[54]. Yorulmaz, U., et al., Vibrational and mechanical properties of single layer MXene structures: a first-principles investigation. 2016. **27**(33): p. 335702.

[55]. Cheng, R., et al., MXenes induce epitaxial growth of size-controlled noble nanometals: A case study for surface enhanced Raman scattering (SERS). 2020. **40**: p. 119-127.

[56]. Zhao, C., M. Zhou, and H.J.A.S.S. Yu, Interfacial combination of Ti3C2Tx MXene with waterborne epoxy anticorrosive coating. 2022. **572**: p. 150894.

[57]. Singh, B., et al., Hydrothermal-assisted synthesis and stability of multifunctional MXene nanobipyramids: structural, chemical, and optical evolution. 2021. **13**(2): p. 3011-3023.

[58]. Hu, T., et al., Chemical origin of termination-functionalized MXenes: Ti3C2 T 2 as a case study. 2017. **121**(35): p. 19254-19261.

[59]. Meshkian, R., et al., Theoretical stability and materials synthesis of a chemically ordered MAX phase, Mo2ScAlC2, and its two-dimensional derivate Mo2ScC2 MXene. 2017. **125**: p. 476-480.

[60]. Zhang, H., et al., Designing flexible 2D transition metal carbides with strain-controllable lithium storage. 2017. **114**(52): p. E11082-E11091.

[61]. Plummer, G., et al., Nanoindentation of monolayer Tin+ 1CnTx MXenes via atomistic simulations: The role of composition and defects on strength. 2019. **157**: p. 168-174.

[62]. Pang, J., et al., Applications of 2D MXenes in energy conversion and storage systems. 2019. **48**(1): p. 72-133.

[63]. Li, Y., et al., In-situ SEM compression of accordion-like multilayer MXenes. 2020. **41**: p. 101054.

[64]. Wang, J., et al., Mechanochemistry-induced biaxial compressive strain engineering in MXenes for boosting lithium storage kinetics. 2021. **87**: p. 106053.

[65]. Zhang, X. and A.J.N. Beyer, Mechanics of free-standing inorganic and molecular 2D materials. 2021. **13**(3): p. 1443-1484.

[66]. Verma, A., et al., A review of composite conducting polymer-based sensors for detection of industrial waste gases. 2023. **5**: p. 100143.

[67]. Aldridge, B.G. and G.A. Stringer, Bridge Circuits: One Topic in the Modular Course in Electronics Instrumentation. 1978.

[68]. Wang, Y., et al., H2S sensing characteristics of Pt-doped α-Fe2O3 thick film sensors. 2007. **125**(1): p. 79-84.

[69]. Gorbova, E., et al., Fundamentals and principles of solid-state electrochemical sensors for high temperature gas detection. 2021. **12**(1): p. 1.

[70]. Park, C.-O., et al., Solid-state electrochemical gas sensors. 2009. **15**: p. 261-284.

[71]. Bakker, E. and M.J.A.c. Telting-Diaz, Electrochemical sensors. 2002. **74**(12): p. 2781-2800.

[72]. Inzelt, G., Electrode potentials, in Handbook of reference electrodes. 2013, Springer. p. 1-24.

[73]. Marković, N., et al., Electrooxidation of CO and H2/CO mixtures on Pt (111) in acid solutions. 1999. **103**(3): p. 487-495.

[74]. Gridchin, V.A., et al. A new piezoresistive pressure sensor on the base of polysilicon thin films with dielectric insulation. in 8th International Forum on Strategic Technology 2013, IFOST 2013-Proceedings. 2013.

[75]. Latif, U. and F.L.J.S. Dickert, Graphene hybrid materials in gas sensing applications. 2015. **15**(12): p. 30504-30524.

[76]. Wang, Y., et al., "Visualization" Gas—Gas Sensors Based on High Performance Novel MXenes Materials. 2024. **20**(2): p. 2305250.

[77]. Pazniak, H., et al., Partially oxidized Ti3C2T x MXenes for fast and selective detection of organic vapors at part-per-million concentrations. 2020. **3**(4): p. 3195-3204.

[78]. Yuan, W., et al., A flexible VOCs sensor based on a 3D Mxene framework with a high sensing performance. 2018. **6**(37): p. 18116-18124.

[79]. Li, N., et al., High-performance humidity sensor based on urchin-like composite of Ti3C2 MXene-derived TiO2 nanowires. 2019. **11**(41): p. 38116-38125.

[80]. Radhakrishnan, S., M. Mathew, and C.S.J.M.A. Rout, Microfluidic sensors based on two-dimensional materials for chemical and biological assessments. 2022. **3**(4): p. 1874-1904.

[81]. Wang, Y., et al., Titanium carbide MXenes mediated in situ reduction allows label-free and visualized nanoplasmonic sensing of silver ions. 2020. **92**(6): p. 4623-4629.

[82]. Shao, H., 2D Ti3C2Tx MXenes for electrochemical energy storage. 2020, Université Paul Sabatier-Toulouse III.

[83]. Li, N., et al., A fully inkjet-printed transparent humidity sensor based on a Ti 3 C 2/Ag hybrid for touchless sensing of finger motion. 2019. **11**(44): p. 21522-21531.

[84]. Wei, H., G. Li, and J. Li, Biomedical Nanozymes: From Diagnostics to Therapeutics. 2023: Springer

Nature.

[85]. Koh, H.-J., et al., Enhanced selectivity of MXene gas sensors through metal ion intercalation: in situ X-ray diffraction study. 2019. **4**(5): p. 1365-1372.

[86]. Seyedin, S., et al., MXene composite and coaxial fibers with high stretchability and conductivity for wearable strain sensing textiles. 2020. **30**(12): p. 1910504.

[87]. Pu, J.-H., et al., Multilayer structured AgNW/WPU-MXene fiber strain sensors with ultrahigh sensitivity and a wide operating range for wearable monitoring and healthcare. 2019. **7**(26): p. 15913-15923.

[88]. Li, H., Z.J.A.a.m. Du, and interfaces, Preparation of a highly sensitive and stretchable strain sensor of MXene/silver nanocomposite-based yarn and wearable applications. 2019. **11**(49): p. 45930-45938.

[89]. Guo, Y., et al., A wearable transient pressure sensor made with MXene nanosheets for sensitive broad-range human–machine interfacing. 2019. **19**(2): p. 1143-1150.

[90]. Yang, Y., et al., Ti3C2Tx MXene-graphene composite films for wearable strain sensors featured with high sensitivity and large range of linear response. 2019. **66**: p. 104134.

[91]. Peng, Y., et al., Ultrasensitive Soft Sensor from Anisotropic Conductive Biphasic Liquid Metal-Polymer Gels. 2024. **36**(8): p. 2305707.

[92]. Chen, L., et al., High-tactile sensitivity of piezoresistive sensors with a micro-crack structure induced by thin film tension. 2019. **40**(9): p. 1519-1521.

[93]. Yang, Y., et al., Strain sensors with a high sensitivity and a wide sensing range based on a Ti3C2Tx (MXene) nanoparticle–nanosheet hybrid network. 2019. **29**(14): p. 1807882.

[94]. Zhang, X., et al., Flexible MXene-decorated fabric with interwoven conductive networks for integrated joule heating, electromagnetic interference shielding, and strain sensing performances. 2020. **12**(12): p. 14459-14467.

[95]. Zhang, H., et al., Wearable pressure sensor array with layer-by-layer assembled MXene nanosheets/Ag nanoflowers for motion monitoring and human–machine interfaces. 2022. **14**(43): p. 48907-48916.

[96]. Li, T., et al., A flexible pressure sensor based on an MXene–textile network structure. 2019. **7**(4): p. 1022-1027.

[97]. Han, S., et al., Tunable Fabrication of Conductive Ti3C2T x MXenes via Inflating a Polyurethane Balloon for Acute Force Sensing. 2020. **36**(5): p. 1298-1304.

[98]. Gao, Y., et al., Microchannel-confined MXene based flexible piezoresistive multifunctional micro-force sensor. 2020. **30**(11): p. 1909603.

[99]. Zhang, Y., et al., Heterogeneous, 3D architecturing of 2D titanium carbide (MXene) for microdroplet manipulation and voice recognition. 2020. **12**(7): p. 8392-8402.

[100]. Gu, J., et al., Extremely Robust and Multifunctional Nanocomposite Fibers for Strain-Unperturbed Textile Electronics. 2023. **35**(15): p. 2209527.

[101]. Han, S., et al., Smart MXene-based Bioelectronic Devices as Wearable Self-powered Health Monitor for Sensing Human Physiological Signals. 2023.

[102]. Dai, T., et al., Bioinspired Dynamic Matrix Based on Developable Structure of MXene-Cellulose Nanofibers (CNF) Soft Actuators. 2024: p. 2400459.

[103]. Zhao, X.-F., et al., A skin-like sensor for intelligent Braille recognition. 2020. **68**: p. 104346.

[104]. Chuang, H., et al., Tear Diagnosis for Diabetic Retinopathy Using an Optoelectrokinetically Driven Bead-based Immunosensor, 20th International Conferenece on Solid-State Sensors, Actuators and Microsystems & Eurosensors XXXIII. 2019.

[105]. Yang, Y., et al., A High-Sensitive Rubber-Based Sensor with Integrated Strain and Humidity Responses Enabled by Bionic Gradient Structure. 2024: p. 2400789.

[106]. Zhang, Q., et al., A Laminated Gravity-Driven Liquid Metal-Doped Hydrogel of Unparalleled Toughness and Conductivity. 2023: p. 2308113.

[107]. Brett, C. and A.M.O.J. Brett, Electrochemistry: principles, methods, and applications. 1993.

[108]. Vidaković, T., M. Christov, and K.J.E.A. Sundmacher, The use of CO stripping for in situ fuel cell catalyst characterization. 2007. **52**(18): p. 5606-5613.

[109]. Yu, X.-f., et al., Monolayer Ti2CO2: a promising candidate for NH3 sensor or capturer with high sensitivity and selectivity. 2015. **7**(24): p. 13707-13713.

[110]. Zhang, Q., et al., High concentration of Ti3C2T x MXene in organic solvent. 2021. **15**(3): p. 5249-5262.

[111]. Kumar, R.J.M.C.P., R. kashyap, R. Kumar, D. Kumar, SK Sharma and M. Kumar. 2020. **240**: p. 121922.

[112]. Gouveia, J.D., et al., First-principles calculations on the adsorption behavior of amino acids on a titanium carbide MXene. 2020. **3**(9): p. 5913-5921.

[113]. Liu, N., et al., Tuning Schottky barriers for monolayer GaSe FETs by exploiting a weak Fermi level pinning effect. 2018. **20**(33): p. 21732-21738.

[114]. Xiao, B., et al., MXenes: Reusable materials for NH3 sensor or capturer by controlling the charge injection. 2016. **235**: p. 103-109.

[115]. Wu, M., et al., V2CT x and Ti3C2T x MXenes nanosheets for gas sensing. 2021. **4**(6): p. 6257-6268.

[116]. Sun, S., et al., W18O49/Ti3C2Tx Mxene nanocomposites for highly sensitive acetone gas sensor with low detection limit. 2020. **304**: p. 127274.

[117]. Xia, Q., et al., MXene-based chemical gas sensors: Recent developments and challenges. 2023. **131**: p. 109557.

[118]. Kim, S., et al., Metallic Ti3C2Tx MXene Gas Sensors with Ultrahigh Signal-to-Noise Ratio. ACS Nano 12: 986-993. 2018.

[119]. Schieweck, A., et al., Smart homes and the control of indoor air quality. 2018. **94**: p. 705-718.

[120]. Umar, A., et al., Enhanced NO2 gas sensor device based on supramolecularly assembled polyaniline/silver oxide/graphene oxide composites. 2021. **47**(18): p. 25696-25707.